ACS APPLIED MATERIALS & INTERFACES
Research Article
www.acsami.org

Mechanical Properties of Molybdenum Disulfide and the Effect of Doping: An in Situ TEM Study

Aleksander A. Tedstone,[†] David J. Lewis,[†] Rui Hao,[‡] Shi-Min Mao,[‡] Pascal Bellon,[‡] Robert S. Averback,[‡] Christopher P. Warrens,[§] Kevin R. West,[§] Philip Howard,[§] Sander Gaemers,[∥] Shen J. Dillon,[*,‡] and Paul O'Brien[*,†]

[†]International Centre for Advanced Materials (ICAM; Manchester Hub), Schools of Materials and Chemistry, University of Manchester, Manchester M13 9PL, United Kingdom

[‡]International Centre for Advanced Materials (ICAM; UIUC Spoke), Frederick Seitz Materials Research Laboratory, University of Illinois at Urbana−Champaign 104 South Goodwin Avenue, MC-230, Urbana, Illinois 61801, United States

[§]BP Technology Centre and [∥]Castrol innoVentures, Whitchurch Hill, Pangbourne, Berkshire RG8 7QR, United Kingdom

Ⓢ *Supporting Information*

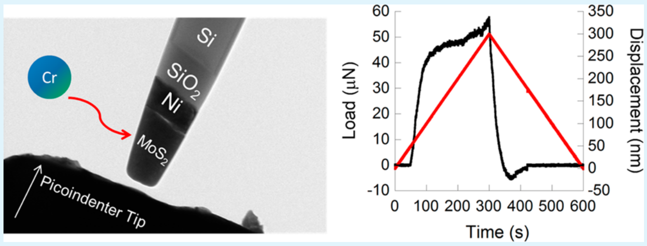

ABSTRACT: Direct observations on nanopillars composed of molybdenum disulfide (MoS_2) and chromium-doped MoS_2 and their response to compressive stress have been made. Time-resolved transmission electron microscopy (TEM) during compression of the submicrometer diameter pillars of MoS_2- and Cr-doped MoS_2 (Cr: 0, 10, and 50 at %) allow the deformation process of the material to be observed and can be directly correlated with mechanical response to applied load. The addition of chromium to the MoS_2 changed the failure mode from plastic deformation to catastrophic brittle fracture, an effect that was more pronounced as chromium content increased.

KEYWORDS: *antiwear films, tribology, in situ electron microscopy, transition metal dichalcogenides*

■ INTRODUCTION

Molybdenum(IV) disulfide (MoS_2) is a ubiquitous solid lubricant[1] along with graphite.[2] These two materials have been used for decades and centuries, respectively, and the concept that they reduce friction because of their intrinsic two-dimensional nature has long been widely appreciated. Lubrication by thin solid films has been studied by macroscopic methods such as tribology, but measurements of their mechanical behavior at the atomic scale are recent.[3,4] Such studies of the interactions between the two-dimensional layers in MoS_2 have, in part, been driven by a burgeoning interest in graphene-like materials.[5] We have recently been interested in two-dimensional materials such as few-layer molybdenum disulfide and few-layer black phosphorus (phosphorene) produced by liquid-phase exfoliation.[6,7]

The nature of the superlubricity of MoS_2 in boundary lubrication arises from its layered crystal structure, in which the three-atom-thick S−Mo−S layers are only weakly bound by van der Waals forces, facilitating shear along the basal plane of the crystals.[8] The interlayer sliding of MoS_2 layers thinned to atomic dimensions by a focused ion beam has been studied by Kim and co-workers.[3] The shear strength under normal load was found to be 25.6 MPa. Tang et al. have directly studied the effect of cleaving MoS_2 pillars on gold with a nanoindenter probe and found that the (200) crystallographic planes deform in a manner dependent upon the number of layers,[4] the mechanical cleavage of two-dimensional crystals has also been studied.[9] These two studies probe the material at the atomic level providing useful information for the study of exfoliation of graphene like materials. Ex situ studies on MoS_2 tend to suggest the validity of these studies, as crystallites have been observed to become oriented by the shear forces experienced in tribological wear.[10,11] Doping of MoS_2 with other transition metals is also of interest and is known to increase the wear resistance of the material without dramatic loss of superlubricity.[12] The effect this transition metal inclusion has on the mechanical failure mode of MoS_2 is unknown. We have studied the effects of the incorporation of chromium into the crystal lattice of molybdenum disulfide. It was found that the highly ordered laminar MoS_2 lattice contracts in the *c* direction and is more disordered upon addition of chromium, decreasing crystal grain size and presenting a network of "cross-linked" lamellae as-evidenced by electron microscopy measurements.[7] The benefit of this morphological change is often an increase in hardness or material persistence at surfaces, which should lead to an increase in wear resistance in tribological applications.[13] We have also been interested in the compression of novel

Received: July 6, 2015
Accepted: August 31, 2015
Published: August 31, 2015

DOI: 10.1021/acsami.5b06055
ACS Appl. Mater. Interfaces 2015, 7, 20829−20834

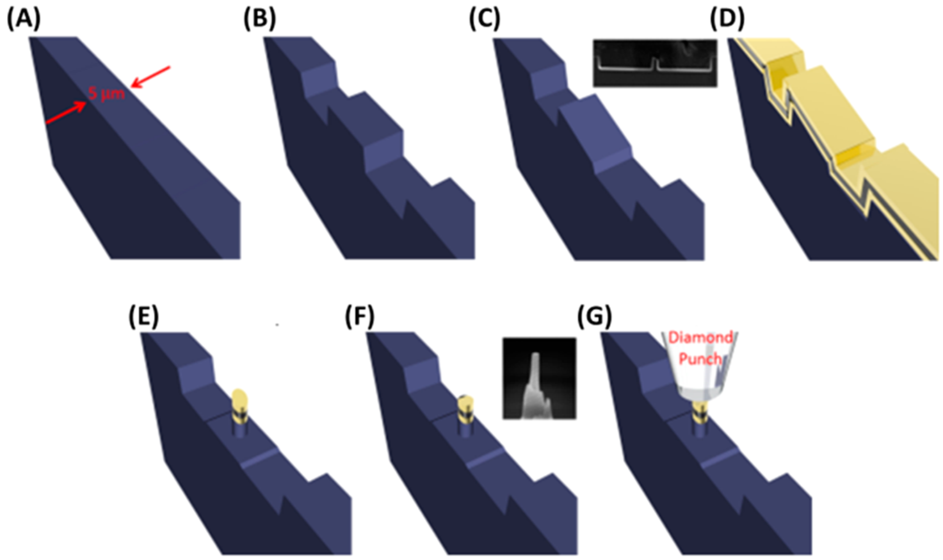

Figure 1. Fabrication scheme for stratified nanopillars. (a) As-supplied silicon substrate, (b) trenches are cut by FIB, (c) creation of angle in central ridge by FIB to induce shear (inset SEM image of an angled pillar), (d) deposition of thin films: thermal silicon oxide growth followed by nickel sputtering and finally MoS_2 by AACVD, (e) creation of nanopillar by FIB, (f) flattening of pillar tip (inset: SEM image of finished pillar), (g) compression by picoindenter tip, as-imaged by TEM.

materials such as metal−organic frameworks at the nanoscale using direct in situ TEM imaging.[14]

In this paper, we report studies of MoS_2 and Cr-doped MoS_2 under compressive stress in a transmission electron microscope, bridging the gap between the nanoscopic/mesoscopic and the macroscopic length scale. This work provides new information about the behavior of this important material, as although there is a precedent for in situ TEM analysis of sliding behavior, compressive experiments that simulate asperity contact in MoS_2 lubricated counterfaces have not been reported. By performing a compression test on a submicrometer diameter pillar of MoS_2- and Cr-doped MoS_2 generated by aerosol-assisted chemical vapor deposition (AACVD), profiles of displacement vs load can be obtained with a concurrent TEM video or image sequence clearly providing a history of how the material fails under stress. The technique simultaneously quantifies material properties (stress/strain curves) and allows a qualitative assessment of structural failure.

■ EXPERIMENTAL SECTION

General. All chemicals and were purchased from Sigma-Aldrich and used without further purification. All reactions were performed in a nitrogen environment using standard Schlenk techniques.

Synthesis of Tetrakis(*N,N*-diethyldithiocarbamato)-molybdenum(IV), MoL_4. Tetrakis(N,N-diethyldithiocarbamato)-molybdenum(IV) was synthesized as described previously.[7] Briefly, to a stirred suspension of molybdenum hexacarbonyl (1.0 g, 3.8 mmol, 1.0 equiv) in acetone (degassed) under N_2, tetraethylthiuram disulfide (2.25 g, 7.6 mmol, 2.0 equiv) was added and brought to reflux for 2 h. After slow cooling to room temperature, a black microcrystalline product precipitated, and was isolated by vacuum filtration, followed by washing with pentane (3 × 20 mL). Mp 119−124 °C. ES-TOF+ m/z: 689 $[M + H]^+$. FT-IR (solid) ν_{max}/cm^{-1}: 2970 (w), 2930 (w), 2869 (w), 1517 (m), 1490 (m), 1454 (m), 1427 (m), 1374 (m), 1352 (m), 1269 (m), 1211 (m), 1145 (m), 1094 (m), 1074 (m), 1001 (m). Anal. Calcd for $C_{20}H_{40}N_4S_8Mo$: C, 34.9%; H, 5.9%; N, 8.1%. Found: C, 34.9%; H, 6.2%; N, 8.0%.

Synthesis of Tris(*N,N*-diethyldithiocarbamato)chromium(III), CrL_3. The chromium(III) complex was synthesized as described previously.[7] Briefly, to a green solution of chromium trichloride hexahydrate (4.0 g, 18 mmol, 1 equiv.) in water (250 mL) adjusted to pH 5 by the addition of concentrated hydrochloric acid was added the monosodium salt of diethyl dithiocarbamate (12.0 g, 54 mmol, 3 equiv.) in portions that effected a color change to blue. Precipitation of a blue solid rapidly followed, which was removed by filtration. The chromium complex was purified using column chromatography on silica eluting chloroform, collecting the rapidly eluted brilliant blue band. The solvent was removed under vacuum to afford the product as an ultramarine solid (1.2 g, 13%). Mp 260−261 °C. ^1H NMR (400 MHz, $CDCl_3$), δ/ppm: 23.9 (s, CH_2), 12.5 (s, CH_2), 0.5 (s, CH_3). ES-TOF+ m/z: 519 $\{M{+}Na\}^+$, 497 $\{M{+}H\}^+$. FT-IR (solid) ν_{max}/cm^{-1}: 2972 (w), 2930 (w), 2868 (w), 1490 (m), 1460 (m), 1450 (m), 1434 (m), 1376 (m), 1357 (m), 1268 (m), 1207 (m), 1141 (m), 1098 (m), 1075 (m), 995 (m). Anal. Calcd for $C_{15}H_{30}N_3S_6Cr$: C, 36.3%; H, 6.1%; N, 8.5%. Found: C, 37.0%; H, 6.6%; N, 8.3%.

General Procedure for Thin Film Deposition. The setup for AACVD in this laboratory has been described in detail previously.[7] Briefly, an aerosol of the precursor feed solution (0% Cr: [MoL_4 (0.2 g, 0.29 mmol)], 10% Cr: [MoL_4 (0.18g, 0.261 mmol), CrL_3 (14 mg, 0.029 mmol)], 50% Cr: [MoL_4 (0.10g, 0.15 mmol), CrL_3 (70 mg, 0.15 mmol)]) dissolved in THF (25 mL) was generated by ultrasonication in a 2 neck RBF. Argon gas at a flow rate of 160 cm^3 min^{-1} was passed through the flask into a quartz tube, containing the substrates positioned in the central region of a Carbolite tube furnace. Coated samples were cooled to room temperature under an argon atmosphere.

Instrumentation. ^1H NMR spectroscopy was performed using a Bruker AVIII400 NMR spectrometer. Electrospray mass spectra were recorded using a Micromass Platform II instrument. Melting points were carried out using a Stuart SMP-10 digital melting point apparatus. FT Infrared absorption spectra were recorded using a Thermo Scientific iD5-ATR spectrometer. Microanalysis was performed using a Thermo Scientific Flash 2000 organic elemental analyzer. Thermogravimetric analyses were performed using a Mettler-Toledo TGA/DSC 1 instrument. Scanning electron microscopy (SEM) was performed using a Philips XL-30 microscope with accelerating voltage of 8−10 kV. Energy-dispersive X-ray (EDX) spectroscopy was performed on the same system at an accelerating voltage of 30 kV using a DX4 EDX detector. Spectra were analyzed using Bruker Esprit software. Samples for SEM imaging were mounted on stubs using conductive Leit carbon tabs (Agar Scientific). Powder X-ray diffraction (pXRD) measurements were made using a Bruker D8 Discover diffractometer using copper K_α radiation (1.54178 Å). Raman spectroscopy was performed using a Renishaw 1000 microscope system equipped with a 50× objective, with solid-state laser excitation

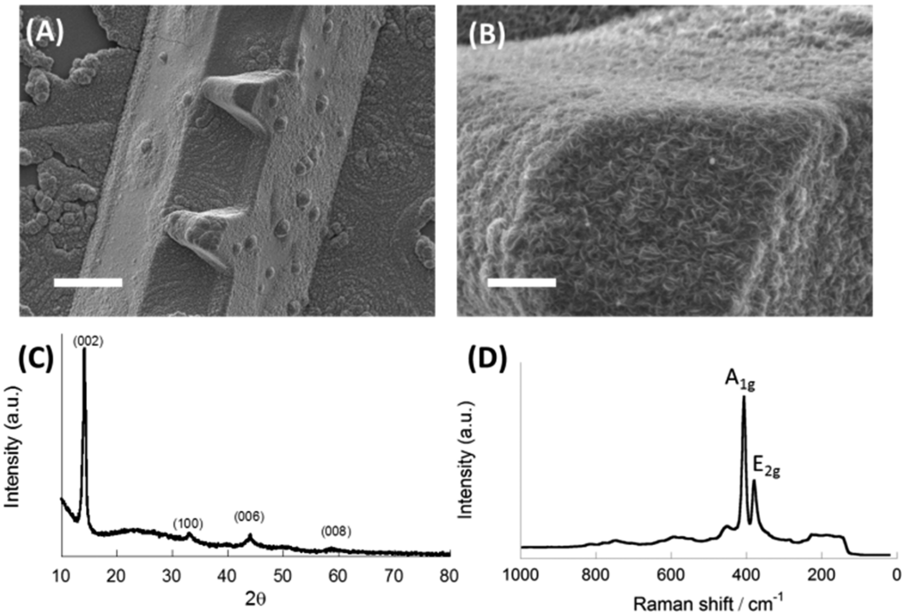

Figure 2. Characterization of nickel substrates as-coated with MoS_2 by AACVD at 450 °C. (a) Top-down secondary electron SEM image (6 kV) of MoS_2 coated nickel substrate. The scale bar represents 20 μm. (b) Top-down secondary electron SEM image (6 kV) of MoS_2-coated nickel substrate at higher magnification. The scale bar represents 5 μm. (c) p-XRD pattern of deposition area around Ni substrate, indexed to 2H-MoS_2. (d) Raman spectrum of a coated substrate, exhibiting A_{1g} and E_{2g} phonon modes characteristic of MoS_2.

(514.5 nm, 20% power). A Hysitron PI 95 TEM PicoIndenter sample holder was used in conjunction with a JEOL 2010 LaB_6 transmission electron microscope to perform micromechanical measurements of frictional materials. The materials of interest were deposited by AACVD onto nickel sputtered silicon substrates with a 1 μm wide central ridge (Hysitron), and a stratified pillar of diameter 250−500 nm was fabricated by focused ion beam milling (FIB) from the ridged section of the substrate (Figure 1). FIB was conducted with a Helios Nanolab 600i system. The pillar was compressed by the diamond punch of the PicoIndenter to generate load vs displacement curves and concurrently imaged to give a video of the pillar through the duration of the compression test. Substrates were mounted in the PicoIndenter with Crystalbond (Agar Scientific). Traditional TEM samples were also prepared by FIB and imaged in the JEOL 2010 LaB_6.

■ RESULTS AND DISCUSSION

Deposition of Doped and Undoped Transition Metal Dichalcogenide (TMDC) Thin Films. The general scheme to produce the stratified pillars for in situ transmission electron microscopy (TEM) imaging of MoS_2 under compressive stress is given in Figure 1. Deposition of molybdenum disulfide onto Si:SiO_2:nickel stratified substrates was achieved by aerosol-assisted chemical vapor deposition (AACVD). Nickel was chosen as the top-layer to simulate the metallic nature of counterfaces commonly found in tribological applications, e.g., engine parts. To prevent nickel reacting with the underlying silicon substrate during MoS_2 growth at 450 °C,[15] we grew a thermal silicon oxide layer on the silicon surface prior to sputtering of a metallic nickel film onto the substrate.

A thin film of MoS_2 was subsequently deposited by AACVD from the tetrakis(*N*,*N*-diethyldithiocarbamato)molybdenum(IV), and characterized by scanning electron microscopy (SEM), energy-dispersive X-ray (EDX) and Raman spectroscopies and powder X-ray diffraction (pXRD) (Figure 2). Inclusion of chromium dopant ions was achieved by including tris(*N*,*N*-diethyldithiocarbamato)chromium(III) in the AACVD precursor solution at the appropriate molar ratio for the desired level of dopant atoms. Thin films (200−500 nm thick) of molybdenum disulfide with 0, 10, and 50 mol % Cr dopant were created.

The Cr content of the chromium-doped MoS_2 films were found to correlate well with the films produced under the deposition conditions reported by Lewis et al.[7] Crystallographic characterization was carried out by pXRD and all films indexed to the pattern of 2H-MoS_2,[16] with a decrease in the intensity and broadening of the (002) diffraction peak concurrent with increasing chromium level (Supporting Information). Raman spectroscopy revealed the characteristic intense A_{1g} and E_{2g} peaks of MoS_2.[17]

Fabrication of Stratified Pillars Terminated with TMDC by Focused Ion Beam (FIB) Milling of Coated Substrates. Stratified pillars of diameter 250−500 nm were fabricated by focused ion beam milling (FIB) from the ridged section of the substrate (Figure 3). A typical stratified pillar consists of a MoS_2 (undoped or Cr-doped) tip, Ni(0) layer,

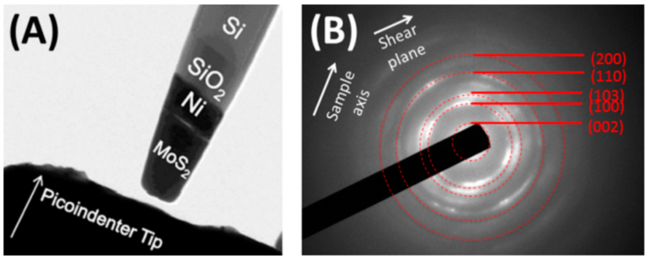

Figure 3. Transmission electron microscopy (TEM) and selected area diffraction (SAED) of a stratified pillar produced in this study. (a) TEM micrograph of a typical final pillar showing the stratified structure with Si, SiO_2, Ni, and MoS_2 layers visible, i.e., a Si:SiO_2:Ni:MoS_2 pillar. The diamond picoindenter can be seen beneath the Si:SiO_2:Ni:MoS_2 pillar. During experiments, the picoindenter punches the pillar, causing compression and finally failure of the material. (b) Typical SAED pattern of a pillar tip that comprises MoS_2, indexed to 2H-MoS_2.

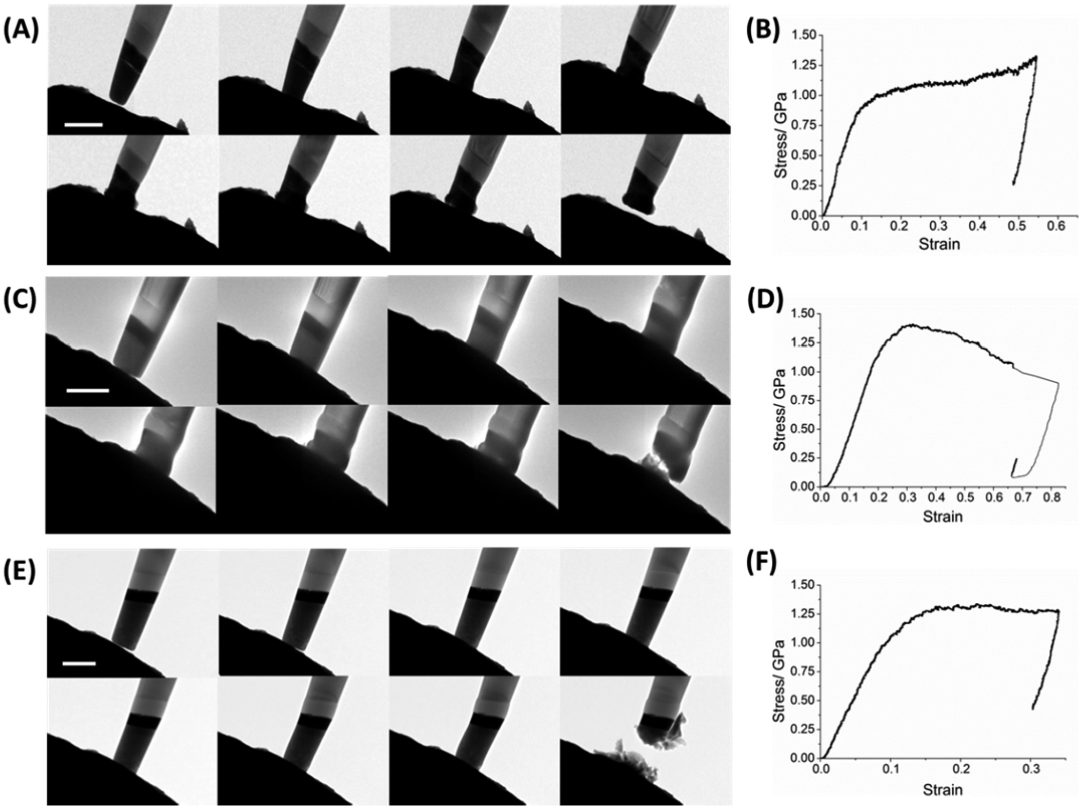

Figure 4. Time-lapse images of micromechanical compression tests; a stratified pillar of MoS_2:Ni:SiO_2:Si (bottom to top) of a diameter in the order of 100−500 nm is compressed at a constant rate of displacement by a Hysitron PicoIndenter tip during bright-field TEM imaging. The scale bars in all figures represent 500 nm and apply to all images. Frames are taken ~60s apart from a continuous video. (a) Tip comprising MoS_2 ,(b) typical stress/strain curve for MoS_2, (c) tip comprising 10 at % Cr-doped MoS_2, (d) typical stress/strain curve for 10 at % Cr-doped MoS_2, (e) tip comprising 50 at % Cr-doped MoS_2, (f) typical stress/strain curve for 50 at % Cr-doped MoS_2.

silicon oxide layer, and silicon base. The layer structure of the pillar did not vary with varying chromium inclusion, as the element was exclusively doped into the layer that constitutes the MoS_2 tip after fabrication is complete. In order to ensure even distribution of the initial compression force, the pillar tip was flattened by FIB milling so that at the moment of contact, both surfaces were parallel.

In Situ TEM Nanomechanical Analysis of Nanopillars under Compression. Pillars were compressed by the diamond punch of a picoindenter within the TEM to generate load vs. displacement curves and videos of the pillar during the compression test. The compression test protocol can be held to simulate asperity contact in dry sliding between MoS_2 lubricated metal interfaces or the boundary lubrication regime of the Stribeck curve (the region in which loads and pressures between tribological interfaces are sufficient to displace any liquid lubricant present) and bring opposing counterfaces into physical contact.[18] Boundary lubrication leads to any protruding parts of the surfaces becoming the active sites for wear as they are subjected to compression at high contact pressures, due to the small surface area of the asperity tip and high mechanical load. As no liquid lubricant is present in this compression test, the influence of adsorbed species from liquid lubricant is neglected. Compression during the test occurs in the direction of the long axis of the pillar, and the angled interfaces in the pillar serve to induce shear failure of the material if it is prone to it. The picoindenter punch is linearly displaced at a constant rate with respect to time, and the force that is required to maintain this regime is recorded to produce curves of stress vs strain (Figure 4). The data set includes the force recorded during retraction of the picoindenter, the rightmost part of each curve should not therefore be interpreted as representing the properties of the material being studied.

The results of nanocompression are shown in Table 1. The mean yield strength of materials increases with the amount of chromium, from 821 ± 141 MPa to 1017 ± 239 MPa for 50 at % Cr-doped MoS_2. The failure mode of the materials, as judged

Table 1. Mechanical Data for MoS_2 Tips Subjected to Nanocompression Testing

Cr dopant (mol %)	yield load (μN)	tip diameter (nm)	yield strength (MPa)	mean yield strength (MPa)	failure mode
0	80	340	881	821 ± 141	bending
	40	235	922		crumpling
	34	256	661		crumpling
5	33	207	981	1010 ± 41	crumpling
	36	210	1039		crumpling
10	140	399	1120	924 ± 277	crumpling
	92	401	728		crumpling/ shear
20	42	230	1011	1047 ± 47	crumpling
	45	230	1083		crumpling
50	133	414	988	1017 ± 239	catastrophic
	135	368	1269		shear
	93	386	795		catastrophic

by visual inspection (Videos S1−S3), range from general crumpling in the case of MoS_2 and 10 at% Cr-doped MoS_2 to shear and snapping, i.e. brittle failure, for 50 at% MoS_2. In general the compressive forces required to elicit plastic deformation in the MoS_2 pillars (821 ± 141 MPa) was generally around 30 times greater on average than the shear forces measured by Oveido et al. for interlayer sliding of MoS_2 in the [120] direction (25.3 ± 0.6 MPa).[3] The MoS_2 used in this study is not orientated as-grown from AACVD. Hence it is likely that the rather more disordered MoS_2 film grown by AACVD gives a greater compressive strength than if an epitaxial layer was deposited by AACVD, i.e., if growth occurred from the surface in the [120] direction solely, the compressive strength that would be dominated by shear failure would be considerably smaller in magnitude, and close to the value determined by Oveido et al.[3] The large compressive strength prior to plastic deformation to align the (002) basal crystallographic plane in MoS_2 with the substrate (vide infra) may confer increased durability to AACVD-grown overlayers in real-world applications such as the coating of engine parts prior to assembly to reduce wear during engine run-in.

The introduction of chromium into the MoS_2 serves to increase the yield strength of the material, but also introduces new brittle failure modes previously unseen in these materials under compressive stress. The introduction of chromium into MoS_2, which is known to lead to disruption of the crystallinity possibly by truncations in the [002] direction.[7] This truncated growth likely accounts for the increase in porosity and fraction of amorphous phase observed in the films (Videos S1−S3). The intrinsic strength enhancement due to chromium doping is more pronounced than indicated by the measured results, but is obscured by the increase in porosity associated with higher dopant concentration. To probe this effect further, SAED was performed in situ on the TMD pillar tips, which gave insight into the effect of the compression on crystallinity. The crystallinity of the chromium-doped MoS_2 tip was dramatically increased by nanocompression, and led to emergence of rings and diffuse spots in the SAED patterns previously composed of diffuse rings indicating polycrystallinity (Figure 5). An increase in long-range order is consistent with a deformation mechanism involving alignment by sliding of lamellae during compression.

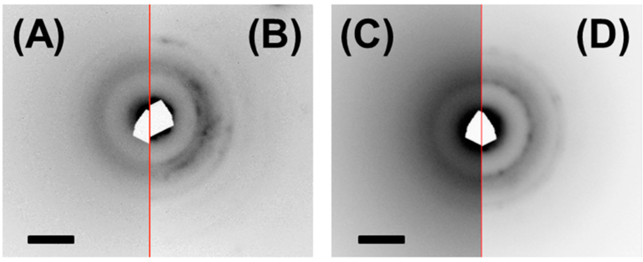

Figure 5. Halved selected-area electron diffraction (SAED) patterns of Cr-doped MoS_2. All scale bars represent 5 nm^{-1}. (a) 10 at % Cr MoS_2 precompression, (b) 10 at % Cr MoS_2 postcompression, (c) 50 at % Cr MoS_2 precompression, (d) 50 at % Cr MoS_2 postcompression.

The presented method is a stepping stone between the nanoscale, mesoscale, and macroscale and will provide further new insights into the in situ behavior of antiwear films under stress, an area that has, until now, remained elusive.

CONCLUSIONS

The imaging and quantification of material failure at the nanoscale is presented for the study of the solid lubricant molybdenum disulfide and its Cr-doped derivatives. The introduction of chromium was found to increase the compressive yield strength of the material potentially offering improved antiwear properties compared with MoS_2. Chromium inclusion dramatically altered the failure mechanism of MoS_2 from a plastic failure mode to a brittle failure mode, an effect that became more pronounced as Cr content increased. Tandem imaging and mechanical analysis affords insight when interpreting regions of the load vs displacement curve that ex situ mechanical testing cannot and thus could potentially be a quantum leap in the way antiwear materials are assessed under stress.

ASSOCIATED CONTENT

Ⓢ Supporting Information

The Supporting Information is available free of charge on the ACS Publications website at DOI: 10.1021/acsami.5b06055.

Powder X-ray diffraction patterns and TEM images (PDF)
Video S1 (AVI)
Video S2 (AVI)
Video S3 (AVI)

AUTHOR INFORMATION

Corresponding Authors

*E-mail: paul.o'brien@manchester.ac.uk.
*E-mail: sdillon@illinois.edu.

Notes

The authors declare no competing financial interest.

ACKNOWLEDGMENTS

The authors acknowledge the funding and support of the BP International Centre for Advanced Materials (BP-ICAM) that facilitated the collaboration in this research. Some of the instrumentation used was funded by the U.K. Engineering and Physical Sciences Research Council (Grant EP/K039547/1). The authors declare no competing financial interests.

REFERENCES

(1) Winer, W. O. Molybdenum disulfide as a lubricant: A review of the fundamental knowledge. *Wear* **1967**, *10*, 422−452.

(2) Scharf, T. W.; Prasad, S. V. Solid lubricants: a review. *J. Mater. Sci.* **2013**, *48*, 511−531.

(3) Oviedo, J. P.; KC, S.; Lu, N.; Wang, J.; Cho, K.; Wallace, R. M.; Kim, M. J. In Situ TEM Characterization of Shear-Stress-Induced Interlayer Sliding in the Cross Section View of Molybdenum Disulfide. *ACS Nano* **2015**, *9*, 1543−1551.

(4) Tang, D.-M.; Kvashnin, D. G.; Najmaei, S.; Bando, Y.; Kimoto, K.; Koskinen, P.; Ajayan, P. M.; Yakobsen, B. I.; Sorokin, P. B.; Lou, J.; Golberg, D. Nanomechanical cleavage of molybdenum disulphide atomic layers. *Nat. Commun.* **2014**, *5*, 3631.

(5) Miro, P.; Audiffred, M.; Heine, T. An atlas of two-dimensional materials. *Chem. Soc. Rev.* **2014**, *43*, 6537−6554.

(6) Brent, J. R.; Savjani, N.; Lewis, E. A.; Haigh, S. J.; Lewis, D. J.; O'Brien, P. Production of Few-Layer Phosphorene by Liquid Exfoliation of Black Phosphorus. *Chem. Commun.* **2014**, *50*, 13338−13341.

(7) Lewis, D. J.; Tedstone, A. A.; Zhong, X. L.; Lewis, E. A.; Rooney, A.; Savjani, N.; Brent, J. R.; Haigh, S. J.; Burke, M. G.; Muryn, C. A.; Raftery, J. M.; Warrens, C.; West, K.; Gaemers, S.; O'Brien, P. Thin

Films of Molybdenum Disulfide Doped with Chromium by Aerosol-Assisted Chemical Vapour Deposition (AACVD). *Chem. Mater.* **2015**, *27*, 1367−1374.

(8) Dickinson, R. G.; Pauling, L. The crystal structure of molybdenite. *J. Am. Chem. Soc.* **1923**, *45*, 1466−1471.

(9) Novoselov, K.; Jiang, D.; Schedin, F.; Booth, T. J.; Khotkevich, V. V.; Morosov, S. V.; Geim, A. K. Two-dimensional atomic crystals. *Proc. Natl. Acad. Sci. U. S. A.* **2005**, *102*, 10451−10453.

(10) Martin, J. M.; Donnet, C.; Lemogne, T.; Epicier, T. Superlubricity of Molybdenum-Disulfide. *Phys. Rev. B: Condens. Matter Mater. Phys.* **1993**, *48* (14), 10583−10586.

(11) Martin, J.-M.; Grossiord, C.; Varlot, K.; Vacher, B.; Le Mogne, T.; Yamada, Y. Friction-induced two-dimensional solid films from lubricant additives. Volume 15, Issue 2. *Lubr. Sci.* **2003**, *15*, 119−132.

(12) Stupp, B. C. Synergistic Effects of Metals Co-Sputtered with MoS_2. *Thin Solid Films* **1981**, *84*, 257−266.

(13) Ding, X. Z.; Zeng, X. T.; He, X. Y.; Chen, Z. Tribological properties of Cr- and Ti-doped MoS2 composite coatings under different humidity atmosphere. *Surf. Coat. Technol.* **2010**, *205* (1), 224−231.

(14) Su, Z.; Miao, Y.-R.; Mao, S.-M.; Zhang, G.-H.; Dillon, S.; Miller, J. T.; Suslick, K. S. Compression-Induced Deformation of Individual Metal-Organic Framework Microcrystals. *J. Am. Chem. Soc.* **2015**, *137*, 1750−1753.

(15) Leonard, F.; Talin, A. A. Electrical contacts to one- and two-dimensional nanomaterials. *Nat. Nanotechnol.* **2011**, *6* (12), 773−783.

(16) Joensen, P.; Frindt, R. F.; Morrison, S. R. Single-layer MoS2. *Mater. Res. Bull.* **1986**, *21* (4), 457−461.

(17) Li, H.; Zhang, Q.; Yap, C. C. R.; Tay, B. K.; Edwin, T. H. T.; Olivier, A.; Baillargeat, D. From Bulk to Monolayer MoS2: Evolution of Raman Scattering. *Adv. Funct. Mater.* **2012**, *22* (7), 1385−1390.

(18) Martin, J. M.; Grossiord, C.; Le Mogne, T.; Igarashi, J. Transfer films and friction under boundary lubrication. *Wear* **2000**, *245* (1−2), 107−115.